PCCP

PAPER

View Article Online
View Journal | View Issue

Cite this: *Phys. Chem. Chem. Phys.*, 2014, **16**, 8493

Liquid state dynamic nuclear polarization of ethanol at 3.4 T (95 GHz)

G. H. A. van der Heijden, A. P. M. Kentgens and P. J. M. van Bentum*

Received 12th December 2013,
Accepted 26th February 2014

DOI: 10.1039/c3cp55254c

www.rsc.org/pccp

Dynamic Nuclear Polarization (DNP) in the liquid state has become the focus of attention to improve the NMR sensitivity of mass limited samples. The Overhauser model predicts a fast reduction in DNP enhancement at high magnetic fields where the electron Larmor frequency exceeds the typical inverse correlation time of the magnetic interaction between an unpaired electron spin of a radical and proton spins of the solvent molecules. The Overhauser hard sphere model is able to predict quantitatively the DNP enhancement for water TEMPOL solutions. The increase in temperature due to dielectric heating of the sample acts to reduce the correlation times and allows a substantial Overhauser DNP. In this paper we extend the work done on water towards other small molecules, such as ethanol. Experimentally we observe a similar enhancement for all three proton groups in the ethanol molecule. The classical interpretation of the low field Overhauser experiments on ethanol invokes a very fast anisotropic rotation of the hydrogen bonded TEMPOL–ethanol complex to explain the fast relaxation of the OH proton. Here we will discuss W-band relaxation and DNP enhancement within this classical model. Although the description can be made quantitative, the invoked parameters do not seem to be realistic. We will propose an alternative model based on the dynamic interaction both in free collision and due to modulation of the hydrogen bond length of the complex.

1 Introduction

Dynamic Nuclear Polarization (DNP) has been around for more than half a century since its discovery in 1953.[1] Over the years DNP has proven to be a viable hyper-polarization technique in both solid and liquid state NMR applications. Liquid state Overhauser DNP has the advantage of studying molecules in solution and *in situ* without the need for solid–liquid phase transitions. In principle, high resolution ^{1}H spectra can be obtained with future potential for fast screening of small metabolites. In addition, Overhauser DNP allows us to study, among others, localized water diffusion[2] and the mobility of biomolecules such as membrane lipids and proteins in their natural environment.[3,4] Over the last decade there has been a renewed interest in the field, where the main effort has been to implement Overhauser DNP at higher fields,[5,6] *e.g.* from 15 MHz up to 144 MHz[7,8] and 400 MHz.[9–11]

In the liquid state DNP often water is chosen as a relatively easy 'test' molecule, despite its high dielectric loss factor. The relatively high self diffusion constant gives rise to an efficient polarization transfer between the radicals and the protons. In most cases TEMPOL (4-hydroxy-TEMPO) is chosen as a convenient water soluble radical. However, the more interesting molecules such as urea, pyruvate, glucose, or alanine are larger and have a significantly lower diffusion coefficient and hence a much lower enhancement factor is observed. Another drawback for solvents with higher viscosity than water is that the rotational correlation times are longer which result in shorter nuclear T_1 times. The main problem however is that the reduced mobility of bigger metabolite molecules prevents direct Overhauser DNP at higher fields. For this reason it is commonly preferred to perform the DNP at a suitable low field and shuttle the sample to the NMR magnet for observation. However, this has the disadvantage that the polarization is based on the low field Boltzmann factor and for fast relaxing protons the final observations may not be quantitative.[6,12] Recently, we have shown that at 3.4 T (95 GHz) the measured enhancements in water TEMPOL solutions are in quantitative agreement with Overhauser theory.[8] In a double resonance EPR/NMR setup with a well defined sample droplet we can determine *in situ* the sample temperature, DNP buildup time and enhancement. In combination with temperature dependent relaxation measurement and EPR determination of the Heisenberg exchange rate we can check the consistency between radical induced relaxation and DNP enhancement without introducing *ad hoc* parameters. For water–TEMPOL mixtures we found a good quantitative agreement between theory and measurements at 3.4 T, allowing a maximum enhancement factor of −165 at temperatures approaching the boiling temperature of water.

In this paper we will present similar DNP experiments for neat ethanol with various concentrations of the TEMPOL radical.

Institute for Molecules and Materials, Radboud University Nijmegen, P.O. Box 9010, 6500 GL Nijmegen, The Netherlands. E-mail: j.vanbentum@science.ru.nl

Compared to water, ethanol has much higher viscosity and lower self diffusion coefficient resulting in reduced translational and rotational correlation time constants for the dipolar interactions with the radical. Furthermore, water has only one functional group, *i.e.* a hydroxyl group, whereas ethanol has extra methylene and methyl groups. These groups may have different Overhauser interaction parameters with the radical. For example the methyl group will have an additional rotational degree of freedom and the hydroxy proton can form hydrogen bonds with the TEMPOL molecule. It is not a priori clear whether the different groups can be described by the same simplified Overhauser model with a single correlation time for the interaction dynamics and with a single parameter for the hard sphere interaction distance. Again, we will seek to perform all measurements *in situ* with no additional fitting parameters. We will use literature data for the self-diffusion constant to define the model parameters for molecular translational dynamics. Rotational dynamics and Heisenberg exchange rate of the TEMPOL molecule will be determined from concentration dependent EPR measurements. Longitudinal relaxation measurements as a function of temperature for different TEMPOL concentrations will be compared with predictions from the Overhauser model. Finally, we will compare the predicted DNP enhancement for all protonated groups from the ethanol molecule with experiments.

2 Overhauser DNP

Consider a solution of a neat liquid with a certain concentration of radicals. The interactions between the nuclear spins on the solvent molecules and the unpaired electron spin on the radicals will result in an increase of the nuclear relaxation rate of the solvent. The extra relaxation is a result of the modulation of the local magnetic field of the electron spin at the site of the nuclear spins at the picosecond timescale. The field modulations are predominantly caused by translational motion of the solvent molecules, rotational motion of a labile solvent–radical complex, and relaxation of the electron spin. The cross relaxation between electron and nuclear spins generates both an enhanced nuclear relaxation as well as an enhancement of the nuclear polarization.

$$\varepsilon = -\frac{(w_0 - w_2)}{w_0 + w_1 + w_2 + w^0}\frac{w}{w + w_e}\frac{\gamma_S}{\gamma_I}, \qquad (1)$$

where the various relaxation rates are depicted in Fig. 1. If the relaxation rates are known, the expected enhancement for a particular system can be calculated. This equation is often simplified to three main parameters which contribute to the enhancement; the coupling factor, the leakage factor and the microwave saturation factor. In the case where additional relaxation mechanisms play a role, like for example due to relaxation induced by rotation of radical–solvent complexes, this separation cannot be achieved unambiguously and may actually lead to some confusion. For this reason we prefer the more fundamental expression given above, where the first term in the enhancement is simply given as a ratio between the net cross relaxation and the total nuclear relaxation.

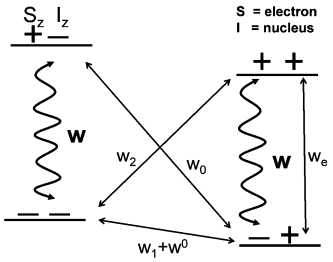

Fig. 1 The energy levels of a proton–electron two-spin system. The longitudinal relaxation rates are the single quantum, w_1, and the intrinsic, w^0, relaxation rates. The cross relaxation rates are the zero quantum, w_0, and the double quantum, w_2. The electron relaxation rate is given by w_e. The applied microwave excitation rate is given by w.

In a previous paper we used the same model to calculate the relaxation rates and the related enhancement. The model was successfully applied to the water–TEMPOL system. The radical induced relaxation was calculated by taking into account both the relaxation caused by translational diffusion and by rotational motion of the labile hydrogen bonded water–TEMPOL complex. For the spectral density function describing the translational motion the hard-sphere force free model by Hwang and Freed was used.[13] The correlation time related to translational diffusion is then given by:

$$\tau_d = \frac{d^2}{D_I + D_S}, \qquad (2)$$

where d is an effective interaction length scale that can be interpreted as an approximate distance of closest approach between the nuclear and electron spins. $D_{I,S}$ are the respective diffusion coefficients for both spins. A significant part of the relaxation for the hydroxyl proton can be caused by the formation of labile hydrogen bonds with the radical. The time constant involved in the complexation τ_m is a combination of the electron spin relaxation time τ_e, the rotational correlation time of the complex τ_r, and the lifetime of the complex τ_l:

$$\tau_m = \left(\frac{1}{\tau_e} + \frac{1}{\tau_r} + \frac{1}{\tau_l}\right)^{-1}. \qquad (3)$$

In the case of ethanol–TEMPOL, we expect that the rotational correlation time dominates the complex relaxation ($\tau_r \ll \tau_e < \tau_l$). The nuclear relaxation times of the neat liquid and the liquid with varying radical concentration can be obtained from standard longitudinal relaxation experiments. A fit to the data within the Overhauser model, using the diffusion data, will give a unique determination of the effective hard sphere interaction distance. If the Overhauser model is quantitatively correct, then the DNP enhancement can be predicted without additional free parameters. For the water–TEMPOL system we found a good agreement with experimental enhancement for all concentrations and temperatures.[8]

3 Materials and methods

The double resonance probe we have used for the DNP experiments is based on a non-radiative dielectric microwave cavity

(95 GHz). Here we will give a short overview of the most important details of the probe. For a more detailed description of the probe the reader is referred to ref. 14. In Fig. 2a a cut away view of the DNP probe is shown. The probe is built from two copper semi-cylindrical parts positioned at a distance less than $\lambda_{mw}/2$. A fused quartz tube is placed through a hole in the copper semi-cylinders, perpendicular to the air slit. In this geometry, the microwave mode is confined by the quartz and the two copper plates. The microwave mode inside the resonator is comparable to that of a metallic TE011 resonator. The most important feature is the dielectric material (fused quartz, Suprasil®15) inside the resonator which reduces the size of the resonator and which results in a higher microwave conversion factor (higher microwave B_1 field amplitude per unit power of radiation). A second benefit of the dielectric resonator is the slightly reduced electric field in the center and hence reduced dielectric heating of the sample. The NMR detection is provided by a simple U-shaped wire loop inserted inside the quartz tube. The coil is part of a $\lambda_{rf}/4$ resonant circuit.

The loaded quality factor of the resonance with a low loss sample is $Q_l = 1300$, which corresponds to an unloaded quality factor $Q_0 = 2100$. For aqueous samples the Q factor is somewhat reduced. The quality factor of the mode, together with its simulated field distribution, allows the calculation of the conversion efficiency in any point of the resonator. For the double resonance probe we find a maximum conversion factor along the axis of the resonator of $B_{1,e} = 1.68\ \mathrm{mT\ W^{-1/2}}$. The maximum effective (circular polarized) MW field is estimated at 47 MHz for a power level of 1 W at the resonator. The intra-cavity proton RF field strength is 330 kHz at 100 W, allowing reasonably sensitive NMR detection for nanoliter sample volumes. The performance of the resonator is strongly affected by the dissipation in the sample, and a compromise must be found between the amount of sample and the resulting conversion factor. For the ethanol solutions investigated in this work, a fused quartz capillary with 200 μm outer- and 100 μm inner-diameters is used as a sample holder. A sample of the radical solution in ethanol was introduced into the capillary as a plug of approximately 1 mm length, sandwiched between two long sections of Fluorinert FC40 (3M Corp.) (see Fig. 2b). The ends of the capillary were sealed with wax. With this restricted sample length we ensure that the sample is positioned in the center part of the resonator where the microwave B_1 field is highest. In this way we avoid complications due to a convolution of the DNP enhancement at the center (giving a negative signal) with the positive signal contributions from protons that are outside the microwave cavity. Also the heating of the sample is nearly homogeneous, making it possible to obtain the sample temperature from the hydroxyl resonance shift.

For the EPR measurements we use a low power CW IMPATT amplifier based heterodyne W-band bridge. The insertion loss of the waveguide was estimated at about 3 dB. A modulation coil and a 3.4 T superconducting Varian magnet with a 45 mm warm bore completed the EPR spectrometer. A small sweep coil was incorporated in the double resonance probe to allow field swept measurements. The EPR spectra are obtained by modulating the static field at about 100 Hz, with an amplitude of 0.15 mT. The DNP experiments were performed using a diode multiplier system driven by a variable frequency synthesizer (VDI). The maximum power output of the oscillator is ~250 mW. The output of the oscillator is amplified by an Extended Interaction Klystron amplifier (CPI Canada, VKB2463) that is capable of generating 100 W microwave power. For the liquid state DNP experiments a maximum power of 1–2 W is needed, corresponding to approximately 300–600 mW in the cavity. During the DNP experiments the microwave power was increased step by step. At each power increment the time that the microwaves are on was increased with logarithmic time increments from ~5 ms up to 5 s. A single pulse experiment was used to obtain the NMR signal. In this way, a single exponential fit of the signal buildup will give both the exponential buildup time and the maximum enhancement. The actual sample temperature was obtained from the temperature dependence of the hydroxyl resonance. The power was increased until the sample evaporated or other instabilities occurred.

The DNP measurements were performed on a Varian Infinity Plus spectrometer. The T_1 relaxation experiments were performed on a commercial Varian probe with VT capabilities. The post processing was done using MatNMR.[16]

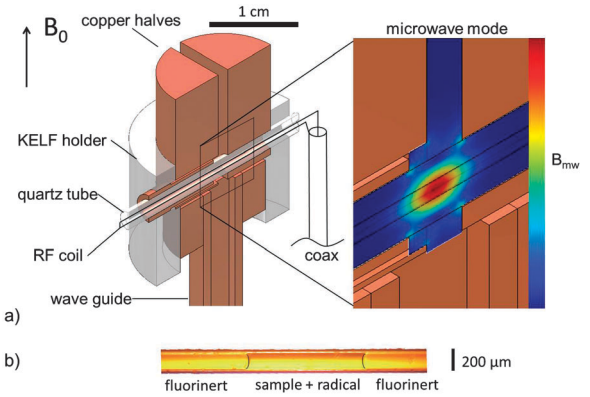

Fig. 2 (a) DNP double resonance probe based on a non-radiative dielectric microwave resonator combined with *in situ* NMR detection. (b) Ethanol sample plug in Fluorinert FC40.

4 Nuclear relaxation

In order to calculate the possible DNP enhancement in the ethanol–TEMPOL system, experimental input is needed for the dynamic model which was introduced in Section 2. To this purpose the T_1 relaxation times of pure ethanol and ethanol with various concentrations of the radical were measured as a function of temperature. The temperature dependence of the relaxation times can be used to identify the dominant relaxation mechanisms. In the case of the water–TEMPOL system, the relaxation times could not be described solely by translational diffusion and a minor contribution to the relaxation due to water–TEMPOL complexation was needed.[8] Second, during the microwave irradiation the temperature of the sample increases,

due to dielectric losses, which in turn modifies the DNP conditions. The experimental enhancements are obtained as a function of microwave power and both polarization and temperature increase simultaneously. The actual temperature is inferred from the OH chemical shift. Independent measurements of the relaxation times as a function of temperature will allow us to check for consistency as the Overhauser model predicts a DNP build-up time equal to the temperature dependent T_1.

In Fig. 3a we have reproduced the experimental values for the self-diffusion constant of neat ethanol at various temperatures.[18] The temperature dependence of the diffusion coefficients can be calculated using the Stokes–Einstein equation, with a molecular radius of 0.195 nm.[19] Over the full range of temperatures, we find a slightly better fit to the data using the Speedy–Angell power law[17] $D = D_0((T/T_S) - 1)^{\alpha}$ with $D_0 = 0.78 \times 10^{-8}$ m^2 s^{-1}, $T_S = 215.05$ K and $\alpha = 2.063$. This fit is indicated with the solid blue curve. The green curve represents the estimated diffusion constant of TEMPOL molecules in ethanol, assuming a hydrodynamic radius of 0.5 nm. The proton T_1 relaxation times are shown in Fig. 3b for neat ethanol without TEMPOL radicals. It can be seen that the relaxation times for the three chemical groups are in the order of 2–4 s depending on temperature. At room temperature the hydroxyl group has a shorter relaxation time as compared to the methyl and methylene groups. As the temperature is increased towards the boiling point ($\sim$78 °C) the relaxation times increase and the difference in relaxation between the three chemical groups decreases. This indicates that the extra relaxation pathway for particularly the hydroxyl proton due to hydrogen bonding between ethanol molecules has a smaller influence at higher temperatures.[20] In Fig. 4a we have plotted the room temperature longitudinal relaxation rate for the distinct protons in ethanol as a function of the radical concentration. For all protons, the relaxation rate increases linearly with radical concentration and for all concentrations, except for the lowest one of 1 mM, the radical induced relaxation is dominant. In panel b we have plotted the Heisenberg exchange rate as a function of the radical concentration at room temperature. These rates are deduced from concentration dependent EPR measurements at room temperature. The hyperfine 14 N coupled triplet can be described assuming an additional line broadening which depends linearly on the radical concentration. The linear fit can be parameterized by 1.01 ± 0.04 MHz mM^{-1}. Note that for the water–TEMPOL system we found a similar behaviour with a Heisenberg exchange rate of 2.27 ± 0.06 MHz mM^{-1}. The reduced Heisenberg exchange rate for the electron spins on the radical molecules can be quantitatively understood in terms of the reduced diffusion coefficient in the more viscous liquid ethanol. In panel c we have plotted the relative shift of the OH resonance at room temperature with respect to the methyl resonance. This upfield resonance shift can be understood as a contact shift induced by hydrogen bonding of the OH proton. This observation indicates the formation of ethanol–TEMPOL complexes. The contact shift can be calculated if we assume that the complex concentration is equal to the radical concentration. The solid line is calculated with a hyperfine coupling constant of the hydroxyl group of -48 μT.[21]

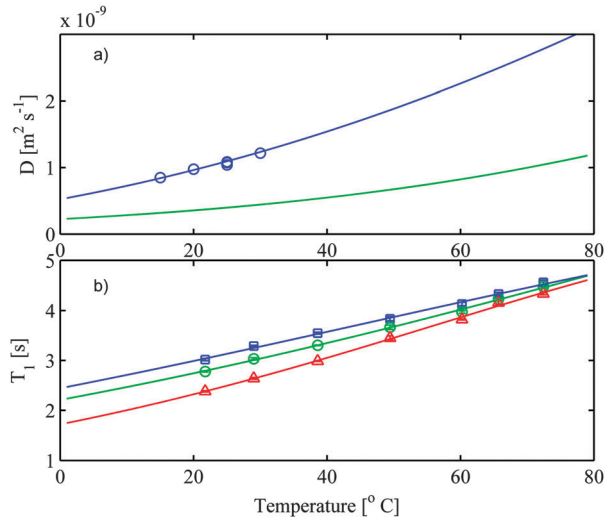

Fig. 3 (a) Self diffusion constant of ethanol (open symbols). The solid lines are fits based on the Speedy–Angell law[17] for both ethanol (blue) and TEMPOL in ethanol (green). (b) The measured T_1 relaxation times of neat ethanol. The three chemical groups are CH_3 (□), CH_2 (○), and OH (△). The solid lines are fits to the data points and are used to parametrize the relaxation of pure ethanol in the model calculations.

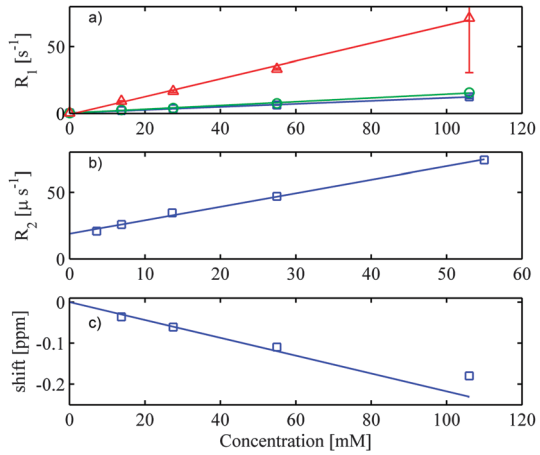

Fig. 4 (a) Relaxation rates of the three groups as a function of TEMPOL concentration at room temperature. Solid lines are a linear fit to the data. (b) TEMPOL transverse relaxation rate R_{2e} as a function of concentration, determined from the EPR line width. (c) The contact shift of the hydroxyl proton as a function of the radical concentration.

5 DNP results

Typical ethanol spectra with and without microwaves are shown in Fig. 5. The TEMPOL concentration is 106 mM. The microwave power at the resonator is estimated at 216 mW. The reference spectrum with microwaves off is multiplied by a factor of 14. The enhancement is the same for all three resonances, which results in an unchanged ratio between the peaks. The hydroxyl resonance shifts upfield as a result of the sample heating during longer microwave irradiation.

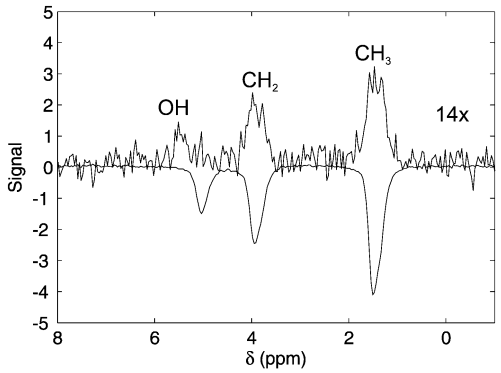

Fig. 5 The ethanol spectrum at thermal equilibrium compared to the polarized spectrum. The polarized spectrum is obtained after 1 s microwave irradiation at a power of 216 mW. The resolution is 0.3 ppm.

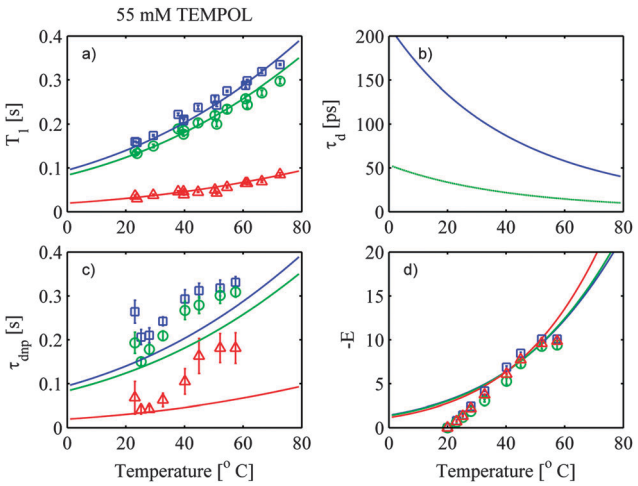

Fig. 6 (a) The measured ^{1}H T_1 relaxation times of ethanol as a function of temperature for a concentration of 55 mM TEMPOL. The solid lines are the calculated relaxation times within the classical model. For parameters see the text. (b) The two dominant timescales related to translational diffusion (blue) and the postulated anisotropic rotation of the hydrogen bonded radical–ethanol complex (green). (c) The measured buildup times of the enhancement for the three distinct protons. The calculated solid lines are as shown in (a). (d) The measured enhancements (CH_3 (□), CH_2 (○), and OH (△)) as a function of temperature compared to the calculated maximum enhancements for the case of full saturation of the radical spin (solid lines).

In Fig. 6 the symbols represent the results obtained at a radical concentration of 55 mM. Panel d shows the power dependent enhancement, while panel c reproduces the experimental buildup time. On the horizontal axis we have chosen to plot the *in situ* measured temperature. The heating above room temperature is in good approximation linear in the applied microwave power. Note that for each increment of the microwave power the buildup time and final enhancement were obtained. The equilibrium temperature of the sample droplet was obtained *via* the OH resonance shift. For comparison the experimental relaxation times as a function of temperature for the same concentration is shown in panel a. An overview of the experiments at other concentrations will appear after the discussion. The solid lines are theoretical fits that we will discuss in more detail in the next section.

The main goal of the present experiment is to check whether the relaxation and DNP enhancement can be described in a self-consistent way within the Overhauser model. In the literature the most common approach is to fit the field dependent relaxation data. Since this is mostly restricted to low magnetic fields it is not always possible to extrapolate the data to relevant fields for modern DNP/NMR experiments.

6 Discussion 1: rotational dynamics

For the discussion we will first follow the traditional approach proposed by the Mueller-Warmuth group to describe relaxation in ethanol radical solutions.[20–25] In this approach one assumes that the methyl and methylene relaxation is fully dominated by translational dynamics. Since the OH relaxation is much faster, it is postulated that TEMPOL–ethanol complexation with fast rotational dynamics will dominate the OH relaxation.[25] A direct comparison with DNP enhancements is generally not possible.

In the following, we will analyse our data within the Mueller-Warmuth model. The relaxation of the CH_3 and CH_2 protons will be used to determine the effective overhauser distance for dipolar translational modulation. The rotational dynamics is then fitted to account for the anomalous OH proton relaxation. Since the viscosity of ethanol is well known, this leads to an estimate of both the bonding distance and the rotational correlation time of the hydrogen bonded complex. We will discuss whether the inferred parameters are realistic for the given van der Waals size of the TEMPOL–ethanol complex. In Fig. 6 panel b, the time constant for translational diffusion (blue line) and the time constant related to the rotation of the solvent–radical complex (green line) are shown. The first was calculated using eqn (2), using the self-diffusion constant as given in Fig. 3a. For the time constant of the complex the dominant contribution is the rotational diffusion (see eqn (3)). The parameter for the distance of closest approach d = 0.42 nm was determined by fitting the methyl relaxation time. The rotational correlation time (green line in Fig. 6b) is calculated using the Stokes–Einstein–Debye equation, assuming a hydrodynamic radius of 0.3 nm and using the temperature dependent viscosity of neat ethanol, corresponding to the self-diffusion data shown in Fig. 3a. In the Stokes–Einstein–Debye equation, the rotational correlation time is given by $\tau_r = \eta_s V/k_B T$, where η_s is the solvent viscosity and V the volume of the solvated TEMPOL molecule. The temperature dependence of the diffusion constants is governed by the Speedy–Angell equation.[17] The timescales decrease with temperature, related to faster dynamics and increased polarization transfer. As can be seen, in order to fit the experimental relaxation data for the OH proton, the rotational correlation time must be significantly shorter than the translational one.

The measured polarization buildup times are shown in panel c (symbols). As can be seen, for low microwave power the buildup times are predicted by the T_1 relaxation time (solid lines). However, at higher microwave powers the buildup times start to deviate from the calculated (isothermal) relaxation

times. In general, the measurement of τ_{DNP} is much more challenging due to the dynamic heating process with thermal time constants of the sample capillary that are also in the 50–100 ms range. Therefore, the error-bars are significantly larger than for T_1 measurements. Nevertheless, the DNP buildup time follows approximately T_1 as expected from theory. In panel d the measured enhancements (symbols) of the three chemical groups are shown together with the calculated enhancements (solid lines). Again, the experimental enhancements are the same for all three chemical groups. With a proper choice of parameters we are able to describe both relaxation and enhancement with satisfactory agreement. For low microwave powers (sample temperatures in the range of 20–30 °C) the measured enhancement is lower than the predicted maximum enhancement since we do not reach full electron spin saturation in this regime.

The relaxation rates are consistent with those in the literature and confirm the faster relaxation of the hydroxyl proton. In the classical literature one relates this effect to hydrogen bonding of the ethanol hydroxyl group to the nitroxide of the TEMPOL.[20–24] It was assumed by Nientiedt *et al.* that at low concentrations of the radical the concentration of this complex is equal to the radical concentration. The exact nature of the free radical, *e.g.* TEMPO or TEMPOL, does not play a role in the relaxivity of the radical.[25]

The enhanced relaxation as a result of the presence of a radical can be calculated by taking into account the two most dominant relaxation contributions: translational diffusion and rotation of a (short lived) TEMPOL–ethanol complex. The intrinsic relaxation rates of neat ethanol were taken as a starting point. The spectral density functions for the translation were based on those of the force-free hard sphere model, and a Lorentzian spectral density function was used for the rotational motion.[8,26] The results for the calculated relaxation times of the ethanol radical solution were compared to the measured relaxation times shown in Fig. 6a. Since the OH group of the ethanol is hydrogen bonded to the nitroxide group, the CH_3 group is located furthest away and we can assume that the CH_3 group has negligible relaxation due to complexation. Therefore, the distance of closest approach for the translational part of the relaxation can be determined from the CH_3 relaxation rate. The best fit parameter for the distance of closest approach is d = 0.42 nm, which is comparable to the values found in the literature of 0.36–0.43 nm.[20,22]

The extra relaxation for the CH_2 and OH groups is introduced *via* the rotation of a labile ethanol–TEMPOL complex. In order to obtain the temperature dependent relaxation the distance was set equal to 0.26 nm and the effective time constant was set to 40 ps. To our knowledge the only data for the distance in the complex for ethanol are obtained by Dally *et al.*[27] They propose a distance of 0.22 nm and a time constant of 50 ps. These results were based on NMRD measurements up to a field of 60 MHz. The traditional approach of Mueller-Warmuth *et al.* is thus also able to reproduce the observed relaxation times and DNP enhancements at 3.4 T as a function of temperature for all three nonequivalent protons in ethanol. However, this cannot be taken as a direct proof for the validity of the various assumptions in this model. In the calculations the enhancement of the hydroxyl group is very dependent on the exact dynamics of the ethanol–TEMPOL complex. A shorter lifetime or faster rotation of the complex will have a large effect on the hydroxyl enhancement. To obtain equal enhancements of all three groups therefore a very distinct choice of the rotational parameters is required. As was indicated in Section 4 the fit to the relaxation data within the present model yielded a rotational correlation time constant for the hydrogen bonded complex at room temperature of 40 ps for an effective electron–proton distance of 0.26 nm. However, from ESR measurements we estimate the rotational time constant of the radical/complex to be about 200 ps. In comparison, for TEMPOL in water we deduced a typical rotation time constant of 80 ps. A slower rotation in the more viscous ethanol thus seems reasonable, and the absolute ratio is consistent with the change in viscosity for the two liquids. It is therefore difficult to embrace the postulate of anomalous fast rotation. Nientiedt *et al.*[25] proposed a linear chain model for the ethanol–radical complex with a very anisotropic rotation dynamics. Such anisotropy might indeed be possible, but support from for example molecular dynamics is still missing. Nientiedt *et al.* indeed caution that their parameters should not be taken as a definitive conclusion. In Fig. 7 we have reproduced a model of the TEMPOL–ethanol complex with a hydrogen bond *via* the OH proton of ethanol. The outer diameter is based on the van der Waals radius of the various atoms. The hydrodynamic shape of this complex can be approximated by an ellipsoid with external diameters of, respectively, 1.3, 0.9 and 0.7 nm. For the calculations shown in Fig. 6 we assumed a rotational correlation time of 40 ps. In the Stokes–Einstein–Debye equation, using the experimental value of the room temperature viscosity in ethanol, this corresponds to an (isotropic) hydrodynamic complexation diameter of 0.6 nm. This diameter seems to be inconsistent with the van der Waals model. An anisotropic rotation as postulated by Nientiedt *et al.* also seems very unlikely. Even if the rotation could be faster, the long axis of the ellipsoid points approximately along the electron–OH proton vector and thus we expect only weak modulations of the magnetic interactions, and thus a negligible contribution to both relaxation and polarization

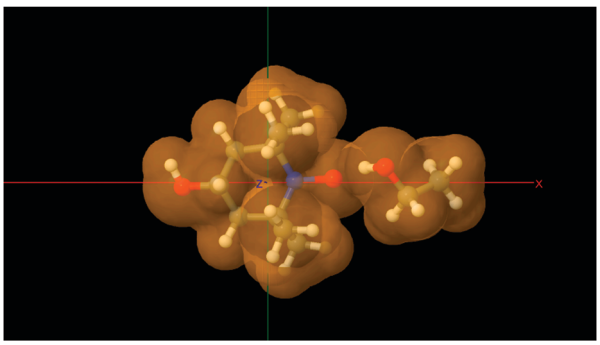

Fig. 7 Schematic representation of a hydrogen bonded TEMPOL–ethanol complex.

enhancement. A second puzzling aspect of the Mueller-Warmuth model is that one has to assume a rather high value for the hard sphere contact distance. For example, the postulated Overhauser contact distance for ethanol–TEMPOL in our calculations (0.42 nm) is almost a factor 2 longer than that found for the water–TEMPOL system (0.24 nm). It is not easy to understand this in terms of the molecular radii, as the complexation distance would then be much shorter than the hard sphere interaction length. For example, in the model of Fig. 7 the minimum electron–proton distance is estimated to be around 0.25 ± 0.05 nm, assuming that the electron spin is localized on the N–O bond in TEMPOL. In summary, although one can indeed obtain quantitative agreement with both the temperature dependent relaxation and DNP enhancement for the different groups, it remains unclear whether this can be viewed as a proof of the underlying model. As discussed, the fast rotation may not be physical and is not consistent with our EPR data where the lines are broader than for the same concentration in water, indicating a slower rotation. Very fast complexation dynamics seems to contradict the observation of contact shifts for the OH proton. Also, it is rather puzzling that the two very different mechanisms with different timescales and interaction distances for the OH proton as compared to the methyl protons end up with nearly identical DNP enhancement factors. As shown by the calculation, it is possible to reproduce such a coincidence, but the choice for all parameters may not be realistic.

7 Discussion 2: dynamic complexation

As an alternative approach we will explore the following scenario: let us assume, as was found for water–TEMPOL, that the translational dynamics has the shortest correlation time and both translation and rotation dynamics will scale proportional to the viscosity of the medium. With the known diffusion constant of ethanol as a function of temperature, and the room temperature EPR calibration point, this fixes the rotation speed. For the viscosity of ethanol a rotational correlation time of about 200 ps at room temperature corresponds to an isotropic hydrodynamic diameter of 1.04 nm. An isotropic hydrodynamic diameter of about 1 nm is not inconsistent with the model shown in Fig. 7. This rather slow rotation cannot explain the magnitude of the observed relaxation, nor the difference in T_1 between CH_2/CH_3 protons and OH. We further assume that complexation occurs on a timescale that is long compared to other dynamics. This seems to be justified by the observed contact shift of the OH proton, indicating a complex formation with a concentration close to that of the radical concentration. On average a rather large fraction of the radicals will be hydrogen bonded to an ethanol OH group. Let us denote this complex fraction by f_c, where $f_c \lesssim 1$. As the OH proton in a complex is much closer to the electron spin in the radical, as compared to CH_2 or CH_3 protons, the radical induced relaxation is much stronger, explaining the disparity in T_1 values. However, for a rotational correlation time of about 200 ps, the contribution to the total relaxation is small and translational dynamics will dominate both relaxation and DNP. We will thus assume that the dominant modulation of the dipolar coupling that leads to longitudinal relaxation is due to translational dynamics, also in the hydrogen bonded complex. A way to visualize this modulation is to assume that the hydrogen bond is relatively weak and the electron–nuclear distance oscillates over a length scale comparable to the hard sphere interaction distance postulated in the Freed model. If viscosity limits the translational motion also in the hydrogen bonded state then the dynamics of the complexation distance modulation occurs at the same time scale as in collisions between free ethanol molecules and radicals in the solution. If both the timescale and the interaction distance is similar then the correlation time is also about the same and the Overhauser model predicts approximately the same relaxation rates, including the cross relaxations, as in the case of a free elastic collision. The correlation times and the spectral density function are then similar for all proton groups in ethanol and thus one would expect a similar DNP enhancement for all protons. The OH proton would on the other hand have a much bigger interaction probability (due to both free collisions and dynamic complexation) and thus a much faster total relaxation. However, the enhancement in the high concentration limit is the same for all protons. For the CH_2/CH_3 protons, the probability for free collision interaction is hindered by the complex formation, the probability for Overhauser contacts are scaled down by a factor $1 - f_c$.

In Fig. 8 we have reproduced the same experimental data as shown in Fig. 6, but now analysed in the present model. The most notable difference is that now the rotational correlation time (green line in panel b) is longer than the translational correlation time τ_d. This rotation dynamics is calculated using the experimentally determined viscosity of neat ethanol, and a

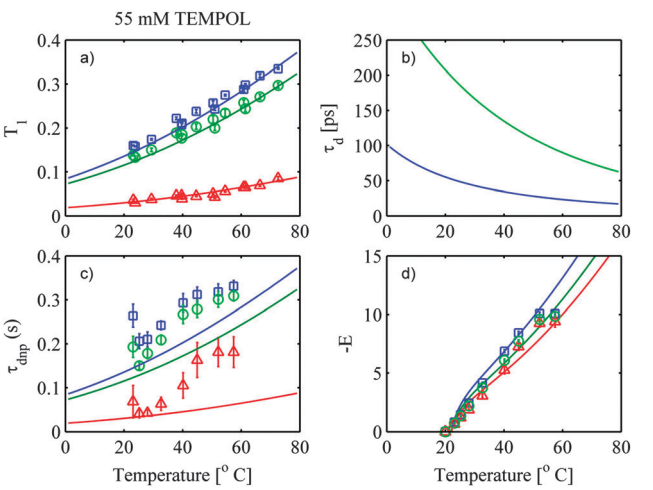

Fig. 8 (a) T_1 relaxation times of ethanol with 55 mM TEMPOL as a function of temperature. The solid lines are calculated using the new model described in the text. (b) Correlation times for translational diffusion (blue) and rotational relaxation of the TEMPOL–ethanol complex (green). (c) The measured buildup times of the enhancement for the three chemical groups (symbols) and the prediction from the model (solid lines). (d) The measured enhancements (symbols) as a function of temperature compared to the predicted enhancements (solid lines), including the effect of (temperature dependent) saturation of the electron spin.

hydrodynamic radius for the TEMPOL–ethanol complex of 0.52 nm derived from the EPR measurements. The dominant relaxation is then caused by translational motion, with a correlation time represented by the blue line in panel b. The translational correlation time is calculated using the known temperature dependent diffusion constant (Fig. 3a) and an assumed hard sphere contact distance d = 0.25 nm. This distance is quite similar to the hard sphere interaction distance that gives an optimal fit for both relaxation and DNP enhancement of the water–TEMPOL system. In order to describe the T_1 and the DNP buildup times we need to make a further assumption about the relative complexation density f_c. For simplicity we will take this parameter as a temperature independent constant f_c = 0.7. Each radical will then have a 70% probability to be in a complex, hydrogen bonded to an ethanol molecule and a 30% probability to be free in solution. In the derivation for the contact shift one generally assumes a complexation fraction $f_c \approx 1$. For CH_2 and CH_3 protons the probability for elastic (Overhauser) collisions is then reduced by a factor 0.3, compared to the situation without complex formation. For the OH proton, the dominant relaxation process is also due to translational interactions with the same dynamics (correlation time τ_d) and in the hard sphere approximation, the same interaction distance d = 0.25 nm, both for the complex dynamics and for the free elastic interaction. As discussed above, this assumption implies that hydrogen bonding does not induce a rigid complex and that the distance modulations are restricted by the same viscosity drag as in the pure liquid. The CH_2/CH_3 protons in the complex are far away from the radical spin and distance modulation does not contribute to the total relaxation. The main result of the complexation *via* the OH proton is thus that all radical induced relaxation rates (zero, single and double quantum cross relaxation) for the OH proton are a factor $1/(1 - f_c)$ higher than for the CH_2/CH_3 protons.

A smaller contribution to the relaxation is induced by the rotation of the complex, as described by the correlation time τ_r. Using a Lorentzian spectral density function and assuming relative distances of 0.29, 0.37 and 0.4 nm of the OH, CH_2 and CH_3 protons to the radical spin we can calculate this additional contribution, which is again highest for the OH proton. The relative distances are loosely inspired by the dimensions of the ethanol molecule. As the contribution to the total relaxation is relatively minor, the exact value should be taken with some caution. With these parameters we find a quite good agreement with the experimental T_1 values as shown with the solid lines in Fig. 8a. The same calculated curves are also shown in panel c and compare reasonably well with the observed DNP buildup times. Finally, the enhancement can now be predicted without further adjustable parameters. In the actual experiment we do not control the temperature but rather increase the microwave power in a linear fashion. The actual temperature of the small sample droplet is determined from the chemical shift of the OH proton relative to the CH_3 resonance, and the results are plotted as a function of this temperature. At low microwave power (small temperature increase of the sample), the electron spin system is not yet saturated and the enhancement curve starts at zero near room temperature. At higher powers, the electron spin system is fully saturated and the curve will approach the theoretical maximum corresponding to the actual temperature of the sample. The solid lines are calculated using a saturation model based on Redfield theory for the case of TEMPOL, using the known g-tensor, hyperfine tensor for the coupling of the electron spin to the ^{14}N nucleus, temperature dependent rotational motion, and experimentally determined Heisenberg exchange. For more details on the theoretical model, see Sezer *et al.*[28] The actual microwave B_1 field is based on the design conversion factor of the resonator, slightly modified to allow for various losses in the waveguide and resonator with an intracavity NMR detection coil. As is clear from the agreement with experimental data, we do find a rather good quantitative agreement between relaxation and DNP enhancement data on ethanol–TEMPOL, as was previously also found for the water–TEMPOL system. Note that the fact that the enhancement for the different protons is quite similar and comes naturally from the model as we assumed that the motional correlation times and interaction hard sphere distances are the same for all protons. However, in the hydrogen bonded complex, the Overhauser interaction with the OH proton is much more frequent and the total relaxation for OH is higher. Nevertheless, as the enhancement is determined by the ratio of the net cross relaxation $(w_0 - w_2)$ to the total relaxation, in the high concentration limit this ratio approaches the same value for all protons in the ethanol molecule.

8 DNP: concentration dependence

The DNP enhancement and buildup times of a range of concentrations from 1 mM to 106 mM were measured. An overview of the results is shown in Fig. 9. The depicted experiments have concentrations of 1, 13.5, 27, and 55 mM. The solid curves are theoretical predictions using the parameters as given in the previous section, except that the concentration is adjusted corresponding to the actual value. It must be noted that the large error-bars in this experiment are due to the fact that the enhancements are close to one, corresponding to a zero signal. In essence, this shows that with the same limited set of parameters we can successfully describe the full concentration range and its temperature dependence for both the relaxation and the dynamic nuclear polarization. In the 1 mM experiment a significant higher enhancement of the hydroxyl proton was measured. The preferred enhancement of the hydroxyl proton is fully reproduced by the theoretical prediction and can be understood in terms of the higher interaction rate for OH protons, which leads to a higher enhancement in the low concentration limit where the radical induced relaxation processes are of the same order of magnitude as the intrinsic longitudinal relaxation of the ethanol molecule. Also, the concentration dependent microwave saturation profile seems to be well reproduced by the model without extra adjustable parameters.

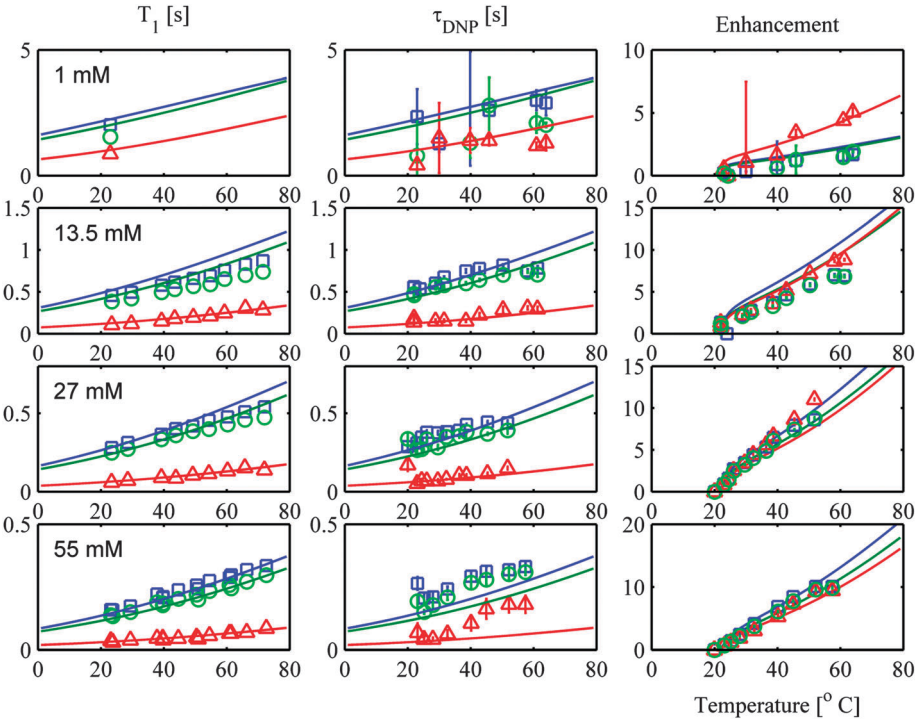

Fig. 9 An overview of the ethanol DNP experiments at different concentrations of 1, 13.5, 27, and 55 mM. The first column represents the experimental T_1 times as a function of the temperature for the four different radical concentrations. The center column shows the buildup times of the polarization as a function of temperature. In the right panels the enhancements as a function of temperature are shown. The solid lines are calculations using the dynamic complexation model. All parameters are fixed (as given in the text), except for the concentration.

9 Conclusions

We have measured the relaxation and dynamic nuclear polarization for the ethanol–TEMPOL system as a function of temperature and concentration. The maximum observed enhancement is about −15, reflecting the higher viscosity of ethanol compared to the previously studied water–TEMPOL system where a maximum enhancement of −165 was observed. The intra-cavity NMR detection of small localized sample droplets allows us to compare the relaxation measurement with the observed enhancement quantitatively as all relevant data are collected *in situ*. The small sample restriction avoids spatial variations of the microwave saturation and temperature, allowing a simplified analysis with a limited set of parameters. We can describe the observations reasonably well within the classical approach where one has to postulate strongly anisotropic rotational dynamics that is faster than the translational interaction. The dynamics are captured in the time constant τ_m, which is basically a combination of the complex lifetime and rotational diffusion. In the literature[22,23,27,29] one assumes that the overall time constant associated with the complex is in the order of 30–50 ps depending on the solvent molecule for the different alcohols. It remains puzzling why such dynamics is much faster in ethanol than in water, where one might expect that the increased viscosity leads to an opposite trend. Also, in these studies, the hard sphere interaction distance is postulated to be much larger than that of the water–TEMPOL system. *A priori* there is no clear physical reason for this as the accessibility for the ethanol protons to the radical electron spin could be quite similar.

We propose an alternative model that includes the molecular hydrogen bonding *via* the OH proton. The internal translational dynamics of the ethanol–TEMPOL complex is assumed to have similar correlation times and hard sphere interaction distances for the free elastic collisions in the solution. The rotational motion is assumed to be isotropic with a reduced dynamics as compared to the water–TEMPOL case, proportional to the increased viscosity of the liquid. This reduced rotational motion is consistent with the EPR measurements that show less motional averaging in the case of ethanol as a solvent. We assume that ethanol–TEMPOL complexation does play an important role, as indicated by the observation of the concentration dependent contact shift of the OH resonance. Assuming a similar translational dynamics and interaction distance both for the hydrogen bonded molecule as for the free elastic collisions we obtain good quantitative agreement between relaxation, dynamic nuclear polarization and theory, assuming basically a single parameter for the hard sphere interaction distance which is very close to that found for water–TEMPOL. A typical complexation fraction of 0.7 is found. Rotational relaxation of the complex provides a minor contribution and is responsible mainly for the observed difference in the relaxation of CH_2 *versus* CH_3 protons.

The dynamic complexation model successfully describes the experimental data for both relaxation and DNP enhancement for all protons in ethanol, without un-physical assumptions.

Further experimental and theoretical work is needed to validate the details of the dynamics.

In the present model we have focussed only on dipolar couplings, as this is generally assumed to be the dominant interaction. Additional scalar couplings may give a small correction to the net interaction, in particular for the nitroxide–OH coupling, leading to a smaller (less negative) enhancement.[30] The fact that we observe similar enhancements for all proton groups in ethanol indicates that scalar couplings can be neglected for the present system.

In combination with the previous work on water–TEMPOL dynamic nuclear polarization, it is clear that the diffusion dynamics is the main key towards efficient Overhauser DNP in the liquid state. This could be realized in high temperature superheated solvents at high pressures or by using supercritical solvents such as CO_2 where one can combine spin densities comparable to that in normal liquids, with diffusion dynamics that may approach that of the gas phase.

Acknowledgements

We are grateful for the technical support from Gerrit Janssen and Jan van Os of the Department for solid state NMR at the Radboud University, and the ACTS-Process On a Chip program for financial support. The double resonance NMR-DNP probe was designed in collaboration with Giuseppe Annino from Pisa, Italy.

References

1 A. W. Overhauser, *Phys. Rev.*, 1953, **92**, 411–415.
2 B. D. Armstrong and S. Han, *J. Am. Chem. Soc.*, 2009, **131**, 4641–4647.
3 R. Kausik and S. Han, *Phys. Chem. Chem. Phys.*, 2011, **13**, 7732–7746.
4 A. Pavlova, E. R. McCarney, D. W. Peterson, F. W. Dahlquist, J. Lew and S. Han, *Phys. Chem. Chem. Phys.*, 2009, **11**, 6833–6839.
5 P. Hoefer, P. Carl, G. Guthausen, T. Prisner, M. Reese, T. Carlomagno, C. Griesinger and M. Bennati, *Appl. Magn. Reson.*, **34**, 393–398.
6 C. Griesinger, M. Bennati, H. Vieth, C. Luchinat, G. Parigi, P. Hoefer, F. Engelke, S. Glaser, V. Denysenkov and T. Prisner, *Prog. Nucl. Magn. Reson. Spectrosc.*, 2012, **64**, 4–28.
7 M. Türke and M. Bennati, *Appl. Magn. Reson.*, 2012, **43**, 129–138.
8 P. van Bentum, G. van der Heijden, J. Villanueva-Garibay and A. Kentgens, *Phys. Chem. Chem. Phys.*, 2011, **13**, 17831–17840.
9 V. Denysenkov, M. J. Prandolini, M. Gafurov, D. Sezer, B. Endeward and T. F. Prisner, *Phys. Chem. Chem. Phys.*, 2010, **12**, 5786–5790.
10 M. Gafurov, V. Denysenkov, M. Prandolini and T. Prisner, *Appl. Magn. Reson.*, 2012, **43**, 119–128.
11 P. Neugebauer, J. Krummenacker, V. P. Denysenkov, G. Parigi, C. Luchinat and T. F. Prisner, *Phys. Chem. Chem. Phys.*, 2013, **15**, 6049.
12 A. Krahn, P. Lottmann, T. Marquardsen, A. Tavernier, M.-T. Turke, M. Reese, A. Leonov, M. Bennati, P. Hoefer, F. Engelke and C. Griesinger, *Phys. Chem. Chem. Phys.*, 2010, **12**, 5830–5840.
13 L.-P. Hwang and J. H. Freed, *J. Chem. Phys.*, 1975, **63**, 4017–4025.
14 G. Annino, J. Villanueva-Garibay, P. van Bentum, A. Klaassen and A. Kentgens, *Appl. Magn. Reson.*, 2010, **37**, 851–864.
15 Polymicro Technologies, Arizona (USA) Suprasil fused Quartz, High purity, ultra low OH, www.molex.com.
16 J. D. van Beek, *J. Magn. Reson.*, 2007, **187**, 19–26.
17 R. Speedy and C. Angell, *J. Chem. Phys.*, 1976, **65**, 851.
18 P. Tofts, D. Lloyd, C. Clark, G. Barker, G. Parker, P. McConville, C. Baldock and J. Pope, *Magn. Reson. Med.*, 2000, **43**, 368–374.
19 B. R. Hammond and R. H. Stokes, *Trans. Faraday Soc.*, 1953, **49**, 890–895.
20 H. Stepankova, J. Englich, J. Stepanek, J. Kohout, M. Pfeffer, J. Cerna, V. Chlan, V. Prochazka and E. Bunyatova, *Acta Phys. Slovaca*, 2006, **56**, 141–144.
21 W. Kolodziejski and K. Zbigniew, *Ber. Bunsen-Ges.*, 1978, **82**, 1312–1314.
22 K. Endo, I. Morishima and T. Yonezawa, *J. Chem. Phys.*, 1977, **67**, 4760–4767.
23 N. Sysoeva, A. Karmilov and A. Buchachenko, *Chem. Phys.*, 1975, **7**, 123–129.
24 J. A. K. Bonesteel, B. Borah and R. D. Bates, *J. Phys. Chem.*, 1984, **88**, 2141–2144.
25 H.-W. Nientiedt, K. Bundfuss and W. Mller-Warmuth, *J. Magn. Reson.*, 1981, **43**, 154–166.
26 M. Bennati, C. Luchinat, G. Parigi and M.-T. Turke, *Phys. Chem. Chem. Phys.*, 2010, **12**, 5902–5910.
27 E. Dally and W. Müller-warmuth, *Ber. Bunsen-Ges.*, 1980, **84**, 260–265.
28 D. Sezer, M. Gafurov, M. Prandolini and V. Denysenkov, *Phys. Chem. Chem. Phys.*, 2009, **11**, 6638.
29 J. L. Russ, J. Gu, K.-H. Tsai, T. Glass, J. C. Duchamp and H. C. Dorn, *J. Am. Chem. Soc.*, 2007, **129**, 7018–7027.
30 J. N. Helbert, E. H. Poindexter and B. E. Wagner, *Chem. Phys. Lett.*, 1977, **52**, 546.

